processes

MDPI

Article

Numerical Simulation of Acid Diversion and Wormhole Propagation Mechanism of Nanoparticle VES Acid in High-Temperature Carbonate Reservoirs

Da Wang [1,2,*], Yunjin Wang [1,*], Puyong Feng [2,3], Yuan Li [1], Kun Zhang [1], Fujian Zhou [1], Fuming Li [4] and Yancai Gao [2]

[1] State Key Laboratory of Petroleum Resources and Prospecting, China University of Petroleum (Beijing), Beijing 102249, China; liyuan2210@163.com (Y.L.); kun_123@foxmail.com (K.Z.); zhoufj@cup.edu.cn (F.Z.)
[2] Production Optimization Research Institute, China Oilfield Services Ltd., Tianjin 300450, China; fengpy@cosl.com.cn (P.F.); gaoyc2@cosl.com.cn (Y.G.)
[3] Tianjin Key Laboratory of Offshore Oil Difficult-to-Recover Reserves Exploitation and Low/Negative Carbon, Tianjin 300450, China
[4] Completion and Workover Department, CNOOC Iraq Ltd., Missan 62001, Iraq; lifm2@cnooc.com.cn
* Correspondence: wangdacup@163.com (D.W.); yunjingwang112@foxmail.com (Y.W.)

Abstract: Uniform acid distribution is a critical challenge and a key factor for the successful acidizing of carbonate reservoirs. Previous experimental studies have shown that nanoparticles can enhance the viscosity and thermal resistance of viscoelastic surfactant (VES) fracturing fluids. However, there has been limited research on the effects of nanoparticles on the wormhole propagation and diversion performance of VES acid. This paper establishes a nanoparticle VES acid rheological model based on rheology experiments, and introduces a porous medium temperature field and nanoparticle adsorption model into a two-scale continuum model to establish a mathematical model for the expansion of wormholes in nanoparticle VES acid. The accuracy of the wormhole model is verified through laboratory experiments. The effects of permeability contrast, initial acid temperature, and nanoparticle adsorption on the diversion performance and wormhole propagation of nanoparticle VES acid are analyzed. The results indicate that nanoparticle VES acid differs from conventional VES acid, with its invaded zone divided into high-viscosity and low-viscosity zones. The presence of the high-viscosity zone allows nanoparticle VES acid to improve wormhole propagation in low-permeability cores by 16.2% compared to conventional VES acid. At 393 K, nanoparticle VES acid has a better diversion effect in carbonate cores with permeability contrast of 10, as the acid fluid flows faster in high-permeability cores, resulting in wormhole shapes with more branches. Numerical model results show that when the permeability contrast is 8, increasing the injection temperature of the acid solution from 293 K to 368 K improves the ability of low-permeability cores by 33.3%. This study establishes a mathematical model for nanoparticle VES acid based on laboratory experiments and numerical simulations, investigates the effects of nanoparticles on VES rheological properties under acidic conditions, and clarifies the wormhole propagation and acid diversion behavior of nanoparticle VES acid, providing guidance for future field applications of this acid.

Keywords: carbonate reservoir; nanoparticle; high temperature; wormhole; diversion

check for updates

Academic Editor: Qingbang Meng

Received: 12 December 2024
Revised: 20 January 2025
Accepted: 21 January 2025
Published: 20 February 2025

Citation: Wang, D.; Wang, Y.; Feng, P.; Li, Y.; Zhang, K.; Zhou, F.; Li, F.; Gao, Y. Numerical Simulation of Acid Diversion and Wormhole Propagation Mechanism of Nanoparticle VES Acid in High-Temperature Carbonate Reservoirs. *Processes* **2025**, *13*, 608. https://doi.org/10.3390/pr13030608

Copyright: © 2025 by the authors. Licensee MDPI, Basel, Switzerland. This article is an open access article distributed under the terms and conditions of the Creative Commons Attribution (CC BY) license (https://creativecommons.org/licenses/by/4.0/).

1. Introduction

Carbonate reservoirs are a promising reservoir characterized by strong heterogeneity similar to unconventional reservoirs [1,2], and uniform acid placement is one of the key technologies for acidizing these reservoirs. The difference between acidizing carbonate reservoirs and sandstone reservoirs lies in the formation of wormholes, which further complicates uniform acid placement. VES acid is a commonly used acid for acid diversion in carbonate reservoirs, but its viscosity decreases rapidly in high-temperature reservoirs. Therefore, improving the diversion ability of VES in high-temperature reservoirs has been a focus of the research in carbonate acidizing.

VES acids commonly use zwitterionic surfactants, such as betaine-type amphoteric surfactants, which exist as individual molecules in fresh acid and are evenly dispersed, resulting in low acid viscosity. As the acid–rock reaction progresses and the pH increases to a certain critical value, the surfactant molecules begin to associate and form micelles. Additionally, divalent metal cations such as Ca^{2+} and Mg^{2+}, produced during acid–rock reactions, shield the charges between molecules and lead to the adsorption of hydrophilic polar groups, transforming spherical or rigid rod-shaped micelles into worm-like micelles. These micelles then merge to form aggregates with a spatial network structure, significantly increasing the spent acid viscosity in high-permeability layers, thus diverting the acid into low-permeability reservoirs, and this diversion effect continues throughout the acidizing process.

Sibarani and Ziauddin [3] experimentally researched the influence of rock heterogeneities on acid diversion, finding that high-permeability zones have the largest pore volume breakthrough and the largest relative pressure buildup during VES acid diversion. Molchanov et al. [4] conducted experiments with a blend of zwitterionic and anionic surfactants, discovering that this combination of VESs could create highly-stable and long-lived worm-like micelles at relatively low concentrations. Zhang et al. [5] found through numerical simulation studies that foam-based VESs could organically combine the diversion ability of foam and VESs, thereby improving the diversion ability and penetration of wormholes. Wang et al. [6] developed a new acid–rock reaction model to analyze the competition between limestone and dolomite during carbonate acidizing. The model simulates wormhole propagation and acidizing efficiency, showing that limestone dominates at lower temperatures, while dolomite becomes more influential as the temperature increases. Additionally, the size, density, and orientation of dolomite affect wormhole formation and propagation.

However, VES acid viscosity rapidly decreases under high-temperature conditions. Some studies have been carried out to improve the diversion performance of VESs, including introducing metal salts, auxiliary surfactants, polymers, and nanoparticles. Nanoparticles, due to their large surface area, can adsorb VES molecules onto the nanoparticles, acting as “cross-linking agents” that extend VES micelles and increase the complexity of their network structure, thereby improving viscosity and enhancing the temperature resistance ability of VES [7]. Hanafy et al. [8] found that nanoparticles at relatively low concentrations can improve the thermal stability and viscosity of cationic VESs, and the shape of nanoparticles has a significant impact on the viscosity of VESs. Philippova et al. [9] demonstrated that the addition of nanoparticles to VES fracturing fluids significantly improves the thermal stability and viscoelasticity of VESs. By altering the surface characteristics of nanoparticles, the sand-carrying ability of nanoparticle-based VES fracturing fluids can also be effectively enhanced. A literature review shows that related studies mainly focus on nanoparticle VES fracturing fluids, with little research on nanoparticle VES acid. The lower pH and higher Ca^{2+} concentration of VES acids significantly affect the adsorption performance of nanoparticles, thereby influencing the expansion and diversion performance of nanoparticle VES acid in wormholes. This necessitates further experimental and numerical studies.

This paper first establishes a rheological model for nanoparticle VES acid based on the rheological characteristics of nanoparticle VES acid at different temperatures and nanoparticle concentrations. Then, a multi-scale, multi-field coupled model of nanoparticle VES is established by coupling the two-scale continuum model, temperature field and adsorption model. The accuracy of this nanoparticle VES acid model is verified through laboratory core flooding experiments. A comparative analysis of the diversion mechanism of nanoparticle VES acid is conducted, and the effects of permeability contrast and temperature on wormhole propagation and diversion performance are studied.

2. Model Description

The two-scale continuum model is the most commonly used model for simulating the propagation of wormholes during acidizing in heterogeneous carbonate formations. This model, first proposed by Panga et al. [10,11], has been developed by several researchers and can accurately describe the propagation of wormholes and the diversion of acid fluids. In this paper, temperature field, nanoparticle adsorption model, and nanoparticle VES acid rheology model are introduced and coupled with this model to study the wormhole propagation and diversion effect of nanoparticle VES acid. When establishing the model, the effects of source sink terms, inertial forces, gravity, and the compressibility of fluids and rocks were neglected.

2.1. Darcy-Scale Model

The two-scale continuum model considers the flow of acid fluid and establishes dynamic boundary conditions to calculate the dissolution of heterogeneous carbonate rocks at each time step, thus obtaining the propagation of wormholes.

At any given reaction moment, the Darcy-scale model uses the continuity equation and the more flexible Darcy–Brinkman equation to describe the micro- and macro-flows of acid fluid in the pore matrix and wormholes:

$$\mu k^{-1} u + \nabla p - \mu \Delta u = 0 \tag{1}$$

$$\frac{\partial}{\partial x}\left(\frac{k}{u}\frac{\partial p}{\partial x}\right) + \frac{\partial}{\partial x}\left(\frac{k}{u}\frac{\partial p}{\partial y}\right) + \frac{\partial}{\partial x}\left(\frac{k}{u}\frac{\partial p}{\partial z}\right) + \frac{\partial \phi}{\partial t} = 0 \tag{2}$$

The reaction of nanoparticle VES acid with carbonate rock causes the concentration of substances in the acid fluid to decrease gradually as the fluid moves. By establishing a reaction equation for nanoparticle VES acid, the distribution of H^+ ions in the acid fluid can be obtained. The distribution of surfactant concentration and the impact of Ca^{2+}, generated in the acid–rock reaction, on the viscosity of the acid fluid are also significant. The following equations for H^+, Ca^{2+}, and VES concentrations can be derived from the reaction equilibrium principle:

$$\nabla\left(uC_f\right) - \nabla\left(\phi D_e \nabla C_f\right) + R(C_s) + \frac{\partial\left(\phi C_f\right)}{\partial t} = 0 \tag{3}$$

$$R(C_s) = k_c\left(C_f - C_s\right) = k_s C_s \tag{4}$$

$$k_c a_v\left(C_f - C_s\right)\alpha = \frac{\partial \phi}{\partial t}\rho_s \tag{5}$$

$$\frac{\partial(\phi C_{Ca^{2+}})}{\partial t} - \nabla(\phi D_e \cdot \nabla C_{Ca^{2+}}) + \nabla(U C_{Ca^{2+}}) + 0.5 k_c a_v\left(C_f - C_s\right) = 0 \tag{6}$$

$$\nabla(\phi D_e \cdot \nabla C_{VES}) - \nabla(U C_{VES}) = \frac{\partial(\varphi C_{VES})}{\partial t} \tag{7}$$

2.2. Pore-Scale Model

The acid fluid dissolution will inevitably change the pore structure and thus affect the related reservoir physical parameters. However, quantitatively characterizing the relationship between these parameters and pore structure is challenging. The two-scale continuum model uses the semi-empirical Garman–Kozeny formula to describe the relationship between porosity, permeability, specific surface area, and changes in pore structure [12]:

$$\begin{cases} \frac{k}{k_0} = \frac{\phi}{\phi_0}\left(\frac{\phi}{\phi_0}\left(\frac{1-\varphi_0}{1-\varphi}\right)\right)^{2\beta} \\ \frac{r_p}{r_{p0}} = \sqrt{\frac{k\phi_0}{\phi k_0}} \\ \frac{a_v}{a_0} = \frac{\phi r_{p0}}{\phi_0 r_p} \end{cases} \tag{8}$$

The mass transfer rate of the acid solution and the solid–liquid surface reaction rate are two decisive parameters that affect the acid–rock reaction rate. The mass transfer coefficient of the acid solution is characterized by the Sherwood number [13,14].

$$Sh = \frac{2k_c r_p}{D_m} = Sh_\infty + \frac{0.7}{h^{1/2}} Re_p^{1/2} Sc^{1/3} \tag{9}$$

The diffusion coefficient is the diffusion rate of reactive ions:

$$D_{\mathrm{eX}} = \alpha_{\mathrm{os}} D_{\mathrm{m}} + \frac{2\lambda_x \left|\vec{U}\right| r_{\mathrm{p}}}{\phi} \tag{10}$$

$$D_{\mathrm{eY}} = \alpha_{\mathrm{os}} D_{\mathrm{m}} + \frac{2\lambda_{\mathrm{T}} \left|\vec{U}\right| r_{\mathrm{p}}}{\phi} \tag{11}$$

2.3. Temperature Field of Porous Medium

The development of wormholes in carbonate reservoirs is not only related to acid–rock reactions and mass transfer but also to temperature [15,16]. The higher the temperature, the faster the diffusion rate of H^+ and the reaction rate with carbonate rocks. The diffusion coefficient and acid–rock reaction rate constant can be expressed by the Arrhenius equation [17], and the values of the relevant parameters are shown in Table 1:

$$D_e = D_e^0 \exp\left(-\frac{\Delta E_D}{RT}\right) \tag{12}$$

$$k_r = k_r^0 \exp\left(-\frac{\Delta E}{RT}\right) \tag{13}$$

Table 1. Reaction parameters of hydrochloric acid with calcium carbonate (Schechter, 1992) [18].

Mineral	k_{r}^0, $\frac{\text{kg moles HCl}}{\mathrm{m}^2\times\mathrm{s}\times\left(\frac{\text{kg moles HCl}}{\mathrm{m}^3\text{ acid solution}}\right)}$	$\frac{\Delta E}{R}$, K	ΔH_{r}, $\frac{\text{KJ}}{\text{mol HCl}}$
Calcium Carbonate	7.314×10^7	7.55×10^3	4.0

The effect of temperature on acid etching wormhole formation mainly comes from two aspects: the heat released by the acid–rock reaction and the cooling effect of the relatively low-temperature acid solution on the reservoir rock. Among these, the impact of heat released by the acid–rock reaction on the temperature field is small, so this study does not consider the influence of the heat released by the acid–rock reaction on the reaction

temperature field. The heat transfer equation for the flow of acid solution in the pore spaces of the reservoir rock is as follows:

$$\overline{\rho c_p}\frac{\partial T}{\partial t} + \rho c_p \nabla \cdot (uT) = \nabla \cdot (\overline{\kappa} \nabla T) \tag{14}$$

2.4. Nanoparticle Adsorption

Silica nanoparticles are transported with the flow of acid into the reservoir porous medium, and this process satisfies the mass conservation equation. Due to their unique physicochemical properties, especially their large specific surface area, nanoparticles can adsorb to pore surfaces through hydrogen bonding and van der Waals forces [19,20]. Experimental studies have shown that nanoparticle adsorption in porous media follows the Langmuir adsorption theory [21]. The transportation behavior of nanoparticles in porous media can be described by the following equation:

$$\frac{\partial(\phi C_{nano})}{\partial t} + \frac{\partial(\rho_s C_{nano,a})}{\partial t} = -\nabla \cdot (uC_{nano}) + \nabla \cdot (\phi D_e \nabla C_{nano}) \tag{15}$$

$$C_{nano,a} = \frac{K_l C_{nano,\max} C_{nano}}{1 + K_l C_{nano}} \tag{16}$$

2.5. Rheological Characteristics of Nanoparticle VES Acid

The viscosity of fresh VES acid is low, but after reacting with the carbonate reservoir, the pH of the acid fluid rises, causing VES to aggregate into spherical micelles. At the same time, H^+ reacts with the carbonate rock minerals, generating divalent cations like Ca^{2+} that further drive the spherical micelles to form rigid rod-like micelles, creating a network structure that significantly increases the viscosity of the spent acid.

Mou et al. [22] developed a rheological model for the VES acid system considering VES concentration, pH, Ca^{2+} concentration, and shear rate:

If $pH \leq$ a

$$\mu = \mu_0 \tag{17}$$

If $pH >$ a

$$\mu_s = \min(\max(\mu_o, 48.567 \times \tilde{r}^{-0.883}), b) \tag{18}$$

$$\mu = \mu_0 + (\mu_s - \mu_0) \times 0.25 \times [erf(c \times (C_{VES} - d) + 1] \times [erf(e \times (C_{CA} - f) + 1] \tag{19}$$

During the flow of the acid in the reservoir, heat exchange occurs between the reservoir rock and the acid solution, leading to an increase in the temperature of the acid solution. Temperature has an important impact on the rheological properties of the acid solution. The viscosity of the VES used in this study increases with temperature. Through laboratory experiments, the relationship between VES acid and temperature is obtained as follows:

$$\begin{aligned}\mu_{\text{ves,T}} &= \mu_o + (\mu_s - \mu_o) \times 0.25 \times [\text{erf}(c \times (C_{VES} - d)) + 1] \\ &\times [\text{erf}(e \times (C_{CA} - f)) + 1] \times 0.0003 \times e^{0.0202T}\end{aligned} \tag{20}$$

According to experimental results, it is found that nanoparticles can effectively increase the viscosity of the spent VES acid. By fitting the rheological experimental data, the relationship between the viscosity of nanoparticle VES acid and nanoparticle concentration can be expressed as follows:

$$\begin{aligned}\mu_{\text{ves-nano,T}} &= \mu_o + (\mu_s - \mu_o) \times 0.25 \times [erf(c \times (C_{VES} - d)) + 1] \times [erf(e \times (C_{CA} - f)) + 1] \\ &\times 0.0003 \times e^{0.0202T} \times [erf(0.175 \times (C_{nano} - 11.4)) + 2]\end{aligned} \tag{21}$$

2.6. Model Structure, Initial and Boundary Conditions

The nanoparticle VES acid model structure and flow pattern are illustrated in Figure 1. Similar to core flow experiments, this model divides the core into an upper low-permeability and lower high-permeability core.

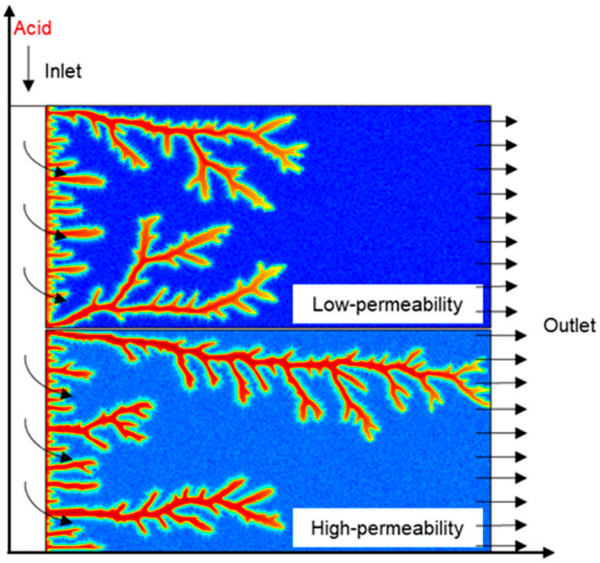


Figure 1. Flow pattern of NP VES acid in the model.

The acid fluid is injected at a constant flow rate q_0, and the exit pressure is set at a constant P_e, while the other boundaries are closed. The continuously injected acid solution almost simultaneously contacts both the high-permeability and low-permeability rock surfaces and enters into the core under the pressure difference. The flow resistance of the high-permeability core is lower, so more acid flows into the high-permeability core, resulting in an imbalance in the amount of acid entering into the high-permeability core and low-permeability core. The acid solution formulation is 20 wt% HCl + 5 wt% VES + 0.05 wt% nanoparticles, with the concentrations of the acid, nanoparticles, and VES maintained constant throughout the injection process. Initially, the pressure inside the system is P_e, and the flow velocity is zero. The main boundary conditions involved in the model are as follows:

$$C_f(x,y,t)\Big|_{t=0} = 0 \tag{22}$$

$$q = \int_0^H u_{x,y}dy\Big|_{x=0} = q_0 \tag{23}$$

$$u_{x,y=0} = 0, v_{x,y=0} = 0 \tag{24}$$

$$u_{x,y=H} = 0, v_{x,y=H} = 0 \tag{25}$$

$$p_{x=L,y} = p_{\text{outlet}} = c \tag{26}$$

The model is solved using Python 3.12 with the finite element method, and the required parameters for the calculations are shown in Table 2. The calculation ideas and processes of the model in this paper are shown in Figure 2.

Table 2. Parameters and values used in the nanoparticle VES acid model.

Parameters	Values	Parameters	Values
u_0	0.005 cm/s	T_l	293 K
Acid density	1 g/cm^3	T_s	393 K
ρ_s	2.20 g/cm^3	α_{os}	0.5
λ_x	0.5	λ_y	0.1
μ_0	0.002 Pa·s	β	1.2
$C_{ves,0}$	5 wt%	Sh	3.66
$C_{H,o}$	6 mol/L	a_{vo}	50 cm^{-1}
D_m	3×10^{-5}cm^2/s	K_l	50 m^3/mol
r_p	0.5 μm	$C_{nano,0}$	5 wt ‰
α	50 g/mol	$C_{nano,max}$	0.0001 mol/kg

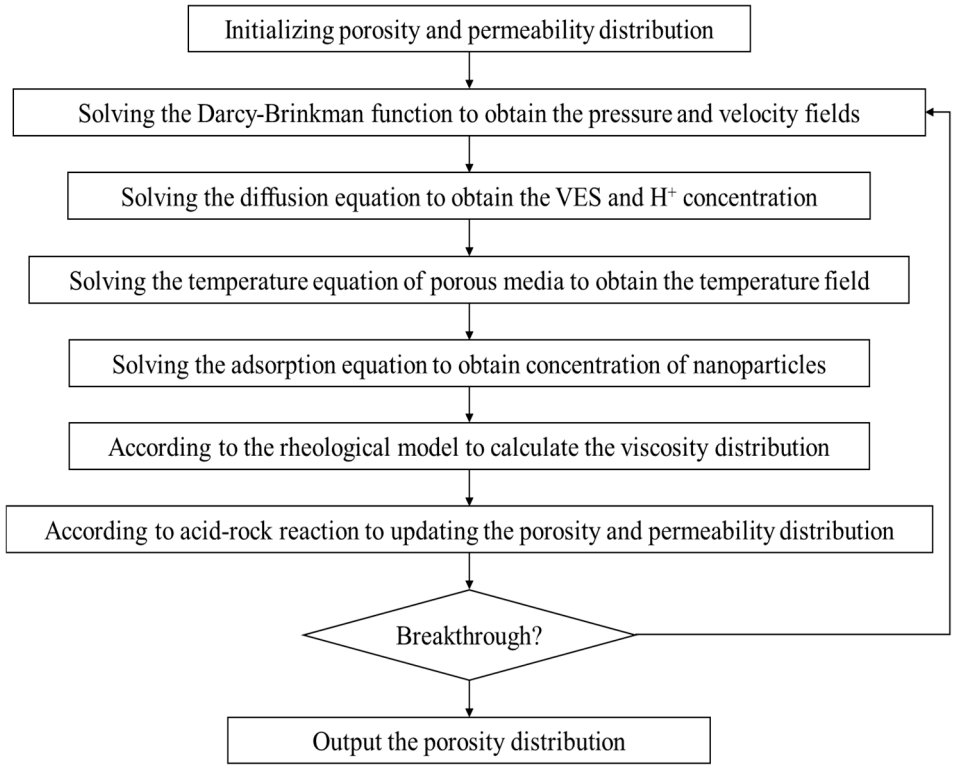


Figure 2. The workflow of mathematical model solution.

3. Result and Discussion

3.1. Wormhole Propagation Pattern

VES acid behaves differently from conventional acid in that, after entering the high-permeability region, the spent acid forms worm-like micelles under the influence of increasing pH and Ca^{2+}, which increases the viscosity of the spent acid and causes subsequent acid fluid to be diverted into the low-permeability zone. Nanoparticle VES acid can further enhance the diversion capability of the acid fluid. This paper compares the behaviors of VES acid and nanoparticle VES acid through laboratory experiments and numerical simulations.

Core flow experiments used 7 cm-long Indiana limestone cores, with permeabilities of approximately 5.3 mD and 40.8 mD (permeability contrast = 8). The acid solution formulation consisted of 20% HCl, 5% VES, 0.05% nanoparticles, and 1% corrosion inhibitor. The SiO_2 nanoparticles (15 nm) were purchased from Jiangsu Qiuyi New Material Company, VES-120 was synthesized by research team, and the anhydrous calcium chloride was purchased from Shanghai McLean Biochemical Technology Co. The back pressure of the core flow system was at 7 MPa to increase system pressure. The parallel core flow

experiments were conducted at a temperature of 363 K. The experimental procedures are the same as those in a paper published by Zhang et al. [23]. The experimental results are shown in Figure 3. The results indicated that the penetration depth of nanoparticle VES acid in the low-permeability core was 4.51 cm.

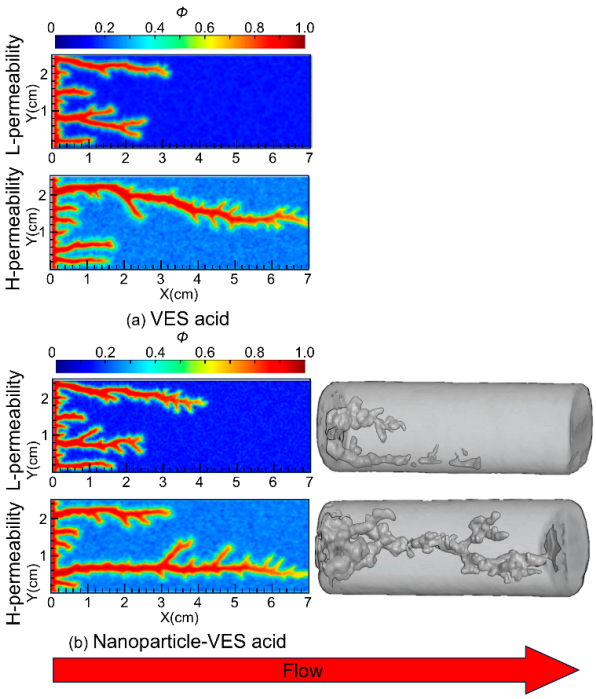


Figure 3. Experimental and numerical simulation results of the wormhole propagation patterns using VES acid and nanoparticle VES acid.

Numerical simulations used cores with the same permeability contrast of 8, with permeabilities of 5 mD and 40 mD. The reservoir temperature was set to 393 K, and the acid solution temperature was 298 K. The simulation results are shown in Figure 3. From the simulation results, it can be seen that in the low-permeability core, the wormhole penetration depth of nanoparticle VES acid is 4.40 cm, compared to 3.28 cm for VES acid. The ratio of wormhole development length in low-permeability to high-permeability cores for both types of VES acid increased from 46.9% to 63.1%, meaning that the wormhole penetration ability of nanoparticle VES acid in low-permeability reservoirs is 16.2% greater than that of conventional VES acid, which is in good agreement with the laboratory experiment results. Both the experimental and simulation results indicate that nanoparticle VES acid can effectively improve the penetration depth of acid etching wormholes in low-permeability zones and improve the effect of uniform acid distribution, thereby helping to solve the problem of the poor stimulation effects of VES acid in low-permeability reservoirs at high temperatures.

Figure 4 shows the distribution of Ca^{2+}, VES molecules, and nanoparticles during the acidizing process for both VES acid and nanoparticle VES acid. The simulation results indicate that the Ca^{2+} produced by the acid–rock reaction of VES acid and nanoparticle VES acid is continuously pushed deeper into the core by the injected acid, resulting in higher concentrations in the deeper parts of the core compared to the injection end. As the VES molecules in the acid solution moves, it undergoes a transformation from spherical micelles to rod-shaped micelles under the influence of Ca^{2+} and pH, forming a spatial network structure. This significantly increases the viscosity of the spent acid and enables the acid diversion.

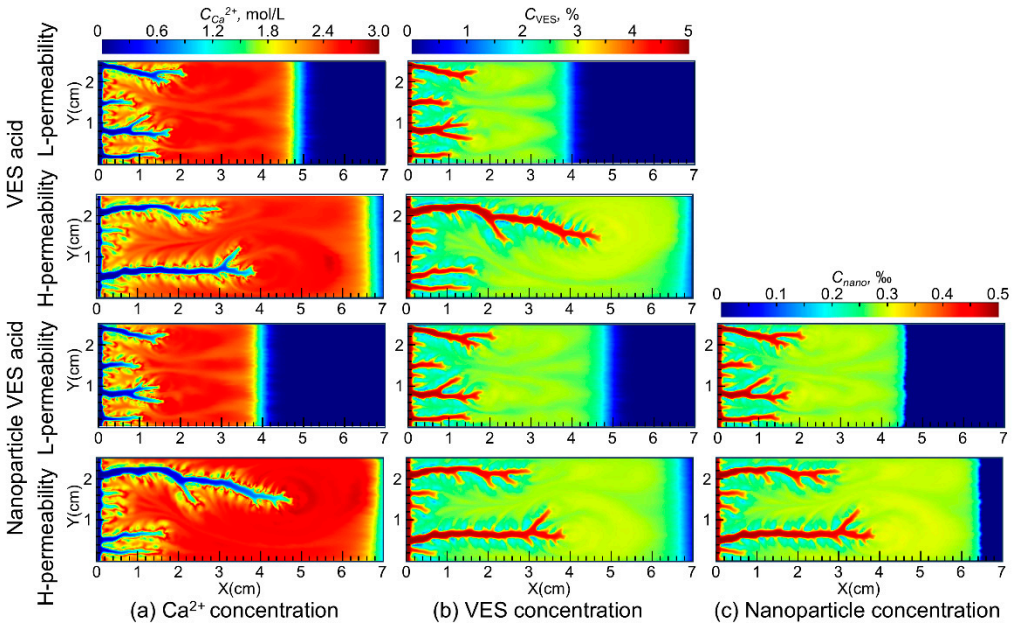


Figure 4. Distribution of Ca^{2+}, VES, and SiO_2 nanoparticles during the wormhole propagation.

The viscosity of the VES system used in this study increases with increasing temperature in the 150 °C VES rheology test. Because the VES spent acid is continuously heated by the reservoir during its flow from the wormhole into the porous medium, its viscosity gradually increases (Figure 5a). In carbonate reservoirs, there is a wormhole zone and a spent-acid-invaded zone during acidizing (Figure 6a). Compared to conventional HCl acid, the spent acid in the VES acid-invaded zone has higher viscosity and greater flow resistance, enabling acid diversion. Numerical simulation of nanoparticle VES acid shows that the concentration of nanoparticles in the acid solution gradually decreases due to adsorption in the porous medium, resulting in a region where only VES spent acid is present without nanoparticles (Figure 4c). In this region, the viscosity of the spent acid is also significantly lower than in areas with nanoparticles (Figure 5b). Therefore, from the comparison of VES acid and nanoparticle VES acid numerical simulation results, it can be seen that, unlike VES acid, the invaded zone of nanoparticle VES acid is subdivided into a high-viscosity zone with nanoparticles and a low-viscosity zone without nanoparticles in the invaded zone (Figure 6b). In the high-viscosity zone, nanoparticle VES acid has higher viscosity than VES acid, while in the low-viscosity zone, after nanoparticles are adsorbed by the formation, the viscosity of nanoparticle VES acid becomes the same as that of conventional VES.

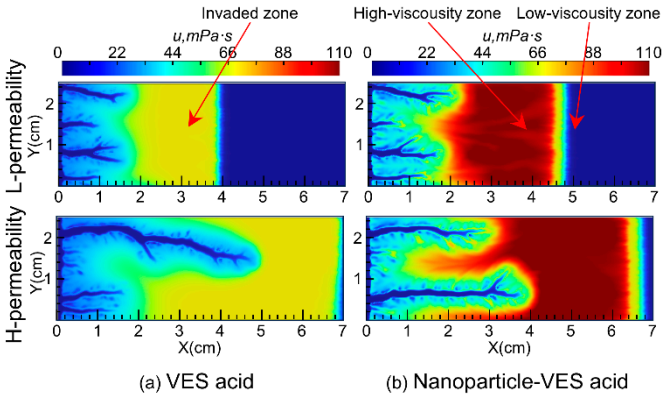


Figure 5. Distribution of fluid viscosity during wormhole propagation.

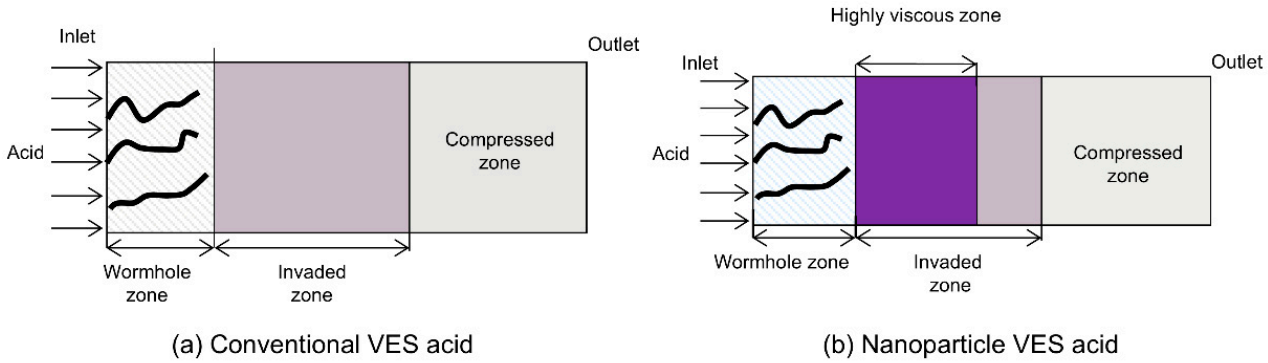


Figure 6. Regional division in acidizing using VES acid and nanoparticle VES acid.

3.2. Permeability Contrast

Permeability contrast is a key indicator for evaluating the heterogeneity of the reservoir and the diversion performance of the acid. The permeability contrast for conventional VES acid in carbonate reservoirs is around 10 [24]. To verify the diversion performance of nanoparticle VES acid, simulations were conducted to study the wormhole propagation in 7 cm-long carbonate cores with permeability contrasts of 5, 8, 10, and 12. The simulation results are shown in Figure 7. The numerical simulation results indicated that as the permeability contrast increased, the length of the wormhole in the low-permeability core gradually decreased.

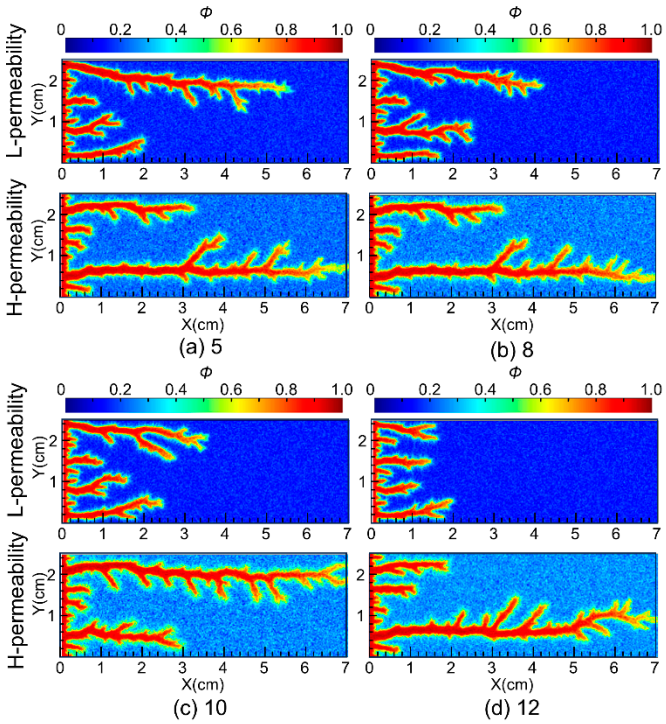


Figure 7. Diverting performances of nanoparticle VES acid at different permeability contrasts.

The ratios of the wormhole length in the low-permeability core to the high-permeability core under the four contrast conditions were 0.82, 0.63, 0.53, and 0.29, as shown in Figure 8. The simulation results suggest that when the permeability contrast of the core is less than 10, nanoparticle VES acid performs well in low-permeability cores. However, when the permeability contrast exceeds 10, the wormhole in the low-permeability core cannot effectively penetrate the damaged zone of the low-permeability core.

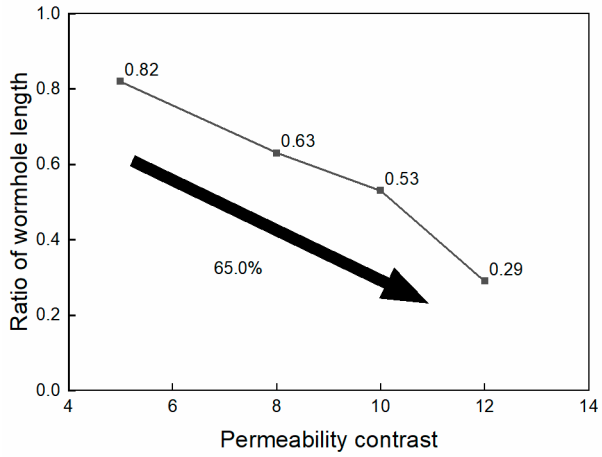


Figure 8. Ratio of wormhole length at different permeability contrasts.

The simulation results indicate that nanoparticle VES acid exhibits excellent diversion performance, which is the result of two factors. First, unlike conventional VES systems, the high-temperature-resistant VES system exhibits an increase in viscosity with rising temperature, allowing the system to maintain a high viscosity even under high-temperature conditions, thereby adapting better to high-temperature environments. As the temperature increases, the viscoelasticity of this system increases, effectively resisting the flow resistance in reservoirs with large permeability contrasts, thereby facilitating better penetration and expansion of the acid into lower permeability zones.

Additionally, one of the key characteristics of nanoparticle VES acid is that the surface properties of the nanoparticles in the acidic environment promote more effective self-assembly of surfactant molecules in the acid solution, forming viscoelastic micelles and a spatial network structure. This significantly enhances the fluid's diversion ability, forming high-viscosity regions, which greatly improves the fluid's diversion capability.

3.3. Temperature Effects

This section investigates the impact of injected acid temperature on wormhole propagation and acid diversion performance, given the unique rheological characteristics of this VES system. The rheological experimental results of the VES system show that its apparent viscosity increases with temperature, making the acid system suitable for matrix acidizing in high-temperature reservoirs. When low-temperature acid is injected into the reservoir, it cools the rock in the wormhole region, which may cause the spent acid viscosity in this region to be lower than that in the deeper regions. However, temperature not only has a significant effect on the apparent viscosity of this acid system but also directly influences the acid–rock reaction rate. Therefore, the impact of temperature on the wormhole propagation and acid diversion performance of nanoparticle VES acid is a complex, multi-factor problem that requires further study.

The distribution of viscosity during wormhole propagation under different injected acid temperatures is shown in Figure 9. The simulation results indicate that, under different injection temperatures, the viscosity of the acid in the wormhole region is lower than in the surrounding external regions. After the nanoparticles are completely adsorbed by the reservoir, the viscosity of the acid decreases further. The reason for the lower viscosity in the wormhole region compared to the adjacent regions is due to the lower Ca^{2+} concentration carried by the acid solution, as well as the higher H^{+} concentration in the wormhole region, which prevents the VES acid from reaching the critical pH value necessary for thickening.

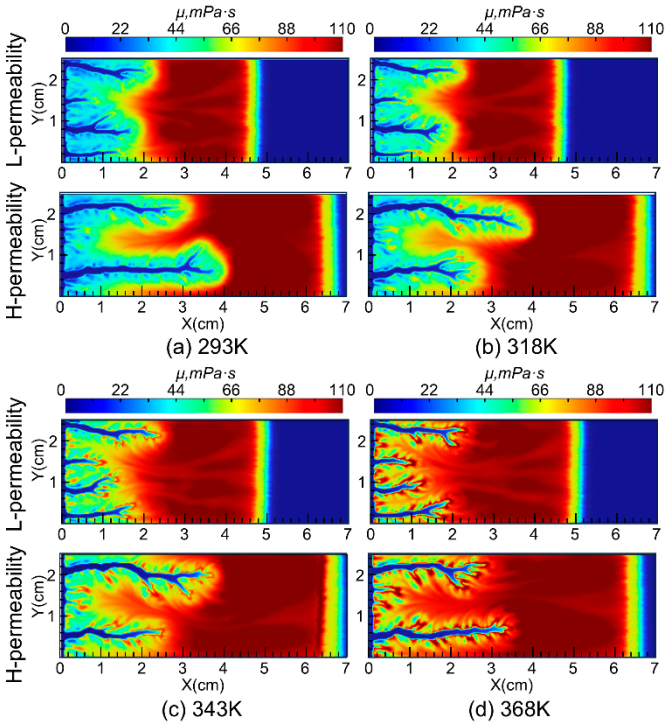


Figure 9. Viscosity distribution during the wormhole propagation.

Additionally, it is related to the unique rheological properties of the VES acid system, which is greatly influenced by temperature. As shown in Figure 10, nanoparticle VES acid at higher injection temperatures results in higher temperatures in the wormhole and surrounding regions. Coupled with the rheological characteristics of the system, the higher temperature increases the viscosity of the spent acid, thereby enhancing its diversion capability.

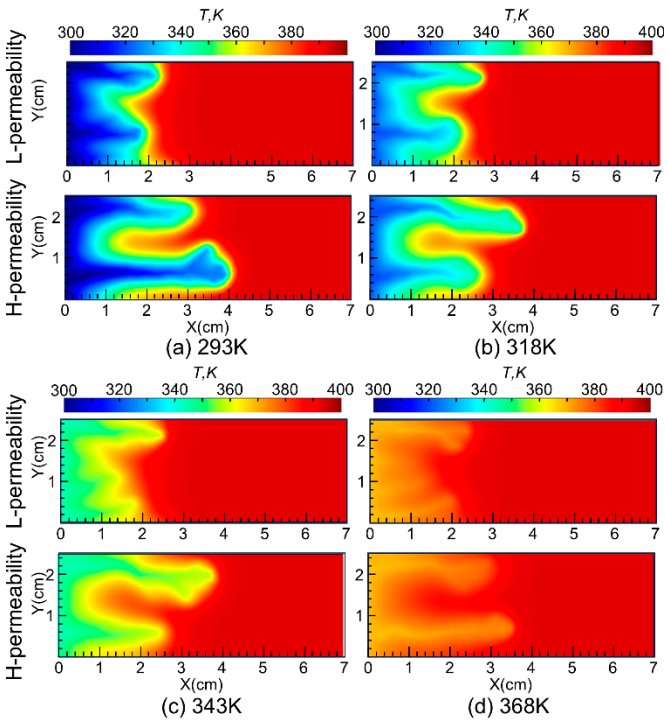


Figure 10. Temperature distribution during the wormhole propagation.

To further investigate the impact of temperature on the diversion performance of nanoparticle VES acid, simulations were conducted at injected acid temperatures of 293 K, 318 K, 343 K, and 368 K. The propagation of wormholes in core samples with a permeability contrast of 8 was simulated, and the results are shown in Figure 11. The simulation results indicate that, within the temperature range of 293 K to 368 K, as the injected acid temperature increases, the wormhole lengths in low-permeability cores gradually increase, suggesting that higher injected acid temperatures are beneficial for the diversion performance of the nanoparticle VES system. Additionally, the simulation results show that the acid-etched wormholes in high-permeability cores are more branched compared to those in low-permeability cores. This is because the acid fluid flows faster in high-permeability cores, allowing it to penetrate a larger area of the porous medium, thus forming more branched wormholes. This is consistent with the results of previous research that the injection rate significantly affects the morphology of wormholes, and wormholes gradually transform from face dissolution to conical wormholes, dominant wormholes, ramified wormholes, and uniform dissolution as the injection rate increases [25].

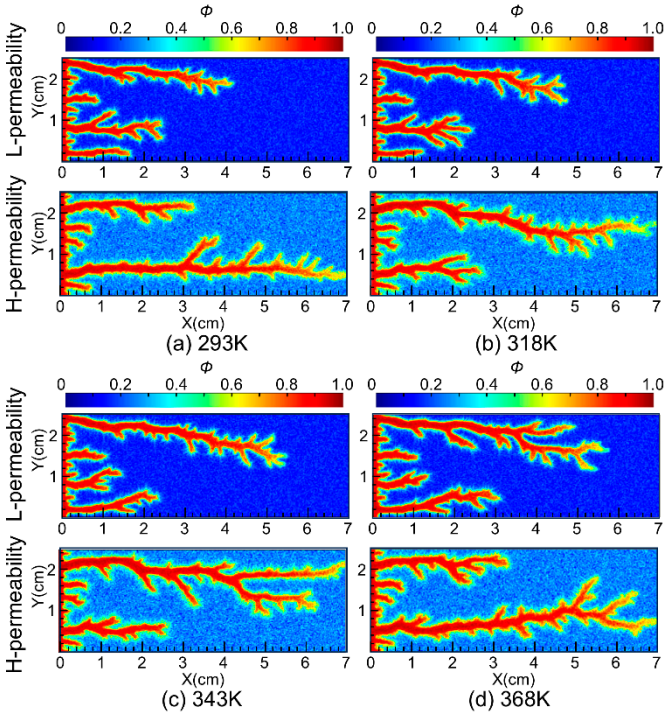


Figure 11. Propagation patterns of wormholes at different temperature.

The ratio of wormhole lengths in high- and low-permeability cores at different injected acid temperatures is shown in Figure 12. As the injected acid temperature increases, the wormhole length in low-permeability cores gradually increases. When the injected acid temperature is 293K, the wormhole length ratio between low-permeability and high-permeability cores is 0.63. When the injected acid temperature is raised to 368K, this ratio reaches 0.84, indicating that the wormhole penetration capacity in low-permeability reservoirs has increased by 33.3%. This suggests that increasing the injected acid temperature helps to enhance the diversion effect of the system.

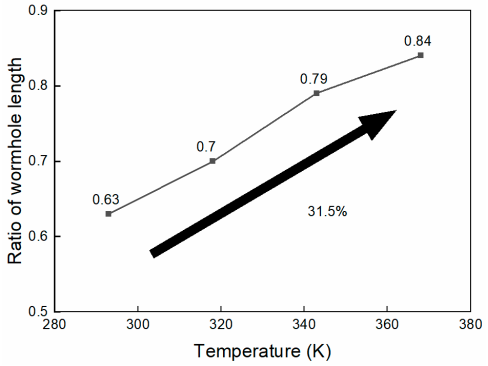


Figure 12. Ratio of wormhole length at different temperature.

4. Conclusions

Based on rheological experimental results, a nanoparticle VES acid wormhole model was established by introducing the nanoparticle VES rheological model, porous media temperature field, and a nanoparticle adsorption model on the basis of a two-scale continuum model. The model was validated through core flooding experiments. The study investigated the propagation patterns of nanoparticle VES acid wormholes and analyzed the effects of acid temperature, nanoparticle adsorption, and core permeability contrast on the wormhole propagation and diversion performance of nanoparticle VES acid. The conclusions are as follows:

(1) Nanoparticle VES acid differs from conventional VES acid. Due to the adsorption effect of nanoparticles, the spent-acid-invaded zone is subdivided into high-viscosity and low-viscosity regions. The presence of the high-viscosity region enables nanoparticle VES acid to enhance the wormhole penetration capacity in low-permeability cores by 16.2% compared to conventional VES acid, thus helping to solve the issue of poor performance of VES acid in low-permeability reservoirs at high temperatures.

(2) At 393 K, nanoparticle VES acid shows good diversion effects for carbonate reservoir cores with a permeability contrast of 10. However, when the permeability contrast is 12, the wormhole length ratio between the low-permeability core and the high-permeability core is only 0.29, indicating poor diversion ability.

(3) In high-permeability cores, the higher acid flow rate results in more complex acid-dissolution paths, leading to the formation of wormholes with more branches.

(4) Numerical modeling results indicate that increasing the injected temperature of the acid fluid can effectively enhance the diversion performance of this VES system. When the permeability contrast is 8, increasing the injected acid temperature from 293K to 368K results in a 33.3% overall increase in wormhole propagation capacity in low-permeability reservoirs.

Author Contributions: Writing—original manuscript, D.W.; writing—review and editing, Y.W.; experiment, Y.L. and K.Z.; supervision, P.F. and F.Z.; formal analysis F.L. and Y.G. All authors have read and agreed to the published version of the manuscript.

Funding: This research is funded by the National Natural Science Foundation of China (No. U23B2084 and No. 52174045) and China Oilfield Services Ltd. (No. E-23257012).

Data Availability Statement: The original contributions presented in this study are included in the article. Further inquiries can be directed to the corresponding authors.

Conflicts of Interest: Authors Da Wang, Puyong Feng and Yancai Gao were employed by the company China Oilfield Services Ltd. Author Fuming Li was employed by the company CNOOC Iraq Ltd. The remaining authors declare that the research was conducted in the absence of any commercial or financial relationships that could be construed as a potential conflict of interest.

Nomenclature

μ	Dynamic viscosity of the fluid
k	Permeability of formation
u	Darcy velocity vector, p is the pressure
Φ	Porosity of formation
C_f	H^+ concentration in acid fluid
D_e	Diffusion coefficient
C_s	H^+ concentration on rock surface
$R(C_s)$	Acid–rock reaction rate
kc	Mass transfer coefficient
k_s	Surface reaction rate constant
a_v	Specific surface of rock
α	Dissolving power
ρ_s	Carbonate rock density
$C_{Ca^{2+}}$	Ca^{2+} concentration
C_{VES}	VES surfactant concentration in acid fluid
k_o	Initial permeability of the formation
Φ_o	Initial porosity of the formation
β	Constant, measured in experiments depending on the structure of the medium
r_p	Pore radius
r_{po}	Initial pore radius
a_{vo}	Initial specific area of the medium.
Sh	Sherwood number
D_m	Acid diffusion coefficient
Sh_∞	Asymptotic Sherwood number
h	Ratio of pore length to pore hydraulic diameter
Re_p	Pore scale Reynolds number, defined by $Re_p = 2\rho u r_p / \mu$
Sc	Schmidt number, given by $S_c = u/\rho D_m$
D_{eX}	Transverse effective diffusion coefficients
D_{eY}	Longitudinal effective diffusion coefficients
λ_x and λ_y	Constants depending on the structure of the porous medium
D_e^0	Diffusion rate constant
$\triangle E$ and $\triangle E_D$	Activation energies
R	Gas constant
T	Absolute temperature
k_r^0	Reaction rate constant
$\overline{\rho \hat{c_p}}$	Average density and specific heat capacity of the rock and fluid
$\hat{c}_p$	Specific heat capacity of the fluid
$\overline{\kappa}$	Average thermal conductivity of the rock and fluid
C_{nano}	Adsorption concentration of nanoparticles, which refers to the number of nanoparticles that can be adsorbed per unit mass of the porous medium
$C_{nano,max}$	Maximum adsorption capacity of nanoparticles
K_l	Langmiur adsorption constant
$C_{nano,a}$	Total adsorption of nanoparticles
μ	Effective viscosity in the porous medium
μ_0	Fresh acid viscosity
a, b, c, d, e, and f	Constants depending on the acid system, which are 0, 2.39, 6, 0.5, 2, and 1.5, respectively, according to the experimental results
$\mu_{ves,T}$	Viscosity of the spent VES acid at temperature T
μ_s	Viscosity of the spent VES acid at 393 K
$u_{ves\text{-}nano,T}$	Viscosity of the spent nanoparticle VES acid at temperature T

References

1. Li, Q.; Li, Q.; Wang, F.; Wu, J.; Wang, Y. The carrying behavior of water-based fracturing fluid in shale reservoir fractures and molecular dynamics of sand-carrying mechanism. *Processes* **2024**, *12*, 2051. [CrossRef]
2. Li, Q.; Li, Q.; Han, Y. A numerical investigation on kick control with the displacement kill method during a well test in a deep-water gas reservoir: A case study. *Processes* **2024**, *12*, 2090. [CrossRef]
3. Sibarani, T.T.; Ziauddin, M. Rock Heterogeneity Effects on Fluid Diversion During Stimulation Treatment. In Proceedings of the SPE Annual Technical Conference and Exhibition, Dubai, United Arab Emirates, 21–23 September 2021; p. D021S036R003.
4. Molchanov, V.; Kuklin, A.; Orekhov, A.; Arkharova, N.; Philippova, O.E. Temporally persistent networks of long-lived mixed wormlike micelles of zwitterionic and anionic surfactants. *J. Mol. Liq.* **2021**, *342*, 116955. [CrossRef]
5. Zhang, L.; Wang, H.; Zhou, F.; Mou, J.J.P. Numerical simulation of wormhole propagation with foamed-viscoelastic-surfactant acid in carbonate acidizing. *Processes* **2023**, *11*, 1839. [CrossRef]
6. Wang, Y.; Zhou, F.; Zhang, Y.; Wang, Y.; Su, H.; Dong, R.; Wang, Q.; Bai, H. Numerical studies and analysis on reaction characteristics of limestone and dolomite in carbonate matrix acidizing. *Geoenergy Sci. Eng.* **2023**, *222*, 211452. [CrossRef]
7. Liu, J.; Liu, P.; Du, J.; Wang, Q.; Chen, X.; Zhao, L. Review on high-temperature-resistant viscoelastic surfactant fracturing fluids: State-of-the-art and perspectives. *Energy Fuels* **2023**, *37*, 9790–9821. [CrossRef]
8. Hanafy, A.; Najem, F.; Nasr-El-Din, H.A. Impact of nanoparticles shape on the VES performance for high temperature applications. In Proceedings of the SPE Western Regional Meeting, Garden Grove, CA, USA, 22–26 April 2018; p. D031S006R007.
9. Philippova, O.E.; Molchanov, V.S. Enhanced rheological properties and performance of viscoelastic surfactant fluids with embedded nanoparticles. *Curr. Opin. Colloid Interface Sci.* **2019**, *43*, 52–62. [CrossRef]
10. Panga, M.K.; Ziauddin, M.; Gandikota, R.; Balakotaiah, V. A new model for predicting wormhole structure and formation in acid stimulation of carbonates. In Proceedings of the SPE International Conference and Exhibition on Formation Damage Control, Lafayette, LA, USA, 26–28 February 2014; p. SPE–86517-MS.
11. Panga, M.K.; Ziauddin, M.; Balakotaiah, V. Two-scale continuum model for simulation of wormholes in carbonate acidization. *AIChE J.* **2005**, *51*, 3231–3248. [CrossRef]
12. Civan, F. Scale effect on porosity and permeability: Kinetics, model, and correlation. *AIChE J.* **2001**, *47*, 271–287. [CrossRef]
13. Balakotaiah, V.; West, D.H. Shape normalization and analysis of the mass transfer controlled regime in catalytic monoliths. *Chem. Eng. Sci.* **2002**, *57*, 1269–1286. [CrossRef]
14. Gupta, N.; Balakotaiah, V. Heat and mass transfer coefficients in catalytic monoliths. *Chem. Eng. Sci.* **2001**, *56*, 4771–4786. [CrossRef]
15. Bousri, A.; Bouhadef, K.; Beji, H.; Bennacer, R.; Nebbali, R. Heat and mass transfer in reactive porous media with local nonequilibrium conditions. *J. Porous Media* **2012**, *15*, 329–341. [CrossRef]
16. Liu, M.; Zhang, S.; Mou, J.; Song, W.; Meng, J. Simulation of temperature field in near-wellbore region in carbonate acidizing. *Ciesc J.* **2013**, *64*, 3542.
17. Arrhenius, S. Über die Reaktionsgeschwindigkeit bei der Inversion von Rohrzucker durch Säuren. *Z. Phys. Chemie* **1889**, *4*, 226–248. [CrossRef]
18. Schechter, R.S. *Oil Well Stimulation*; U.S. Department of Energy Office of Scientific and Technical Information: Oak Ridge, TN, USA, 1992.
19. Betancur, S.; Carrasco-Marín, F.; Pérez-Cadenas, A.F.; Franco, C.A.; Jiménez, J.; Manrique, E.J.; Quintero, H.; Cortés, F.B. Effect of magnetic iron core–carbon shell nanoparticles in chemical enhanced oil recovery for ultralow interfacial tension region. *Energy Fuels* **2019**, *33*, 4158–4168. [CrossRef]
20. Hu, Z.; Zhao, J.; Gao, H.; Nourafkan, E.; Wen, D. Transport and deposition of carbon nanoparticles in saturated porous media. *Energies* **2017**, *10*, 1151. [CrossRef]
21. Yekeen, N.; Al-Yaseri, A.; Idris, A.K.; Khan, J.A. Comparative effect of zirconium oxide (ZrO_2) and silicon dioxide (SiO_2) nanoparticles on the adsorption properties of surfactant-rock system: Equilibrium and thermodynamic analysis. *J. Pet. Sci.Eng.* **2021**, *205*, 108817. [CrossRef]
22. Mou, J.; Liu, M.; Zheng, K.; Zhang, S. Diversion conditions for viscoelastic-surfactant-based self-diversion acid in carbonate acidizing. *SPE Prod. Oper.* **2015**, *30*, 121–129. [CrossRef]
23. Zhang, L.; He, J.; Wang, H.; Li, Z.; Zhou, F.; Mou, J. Experimental investigation on wormhole propagation during foamed-VES acidizing. *J. Pet. Sci. Eng.* **2021**, *198*, 108139. [CrossRef]

24. Al-Ghamdi, A.H.; Mahmoud, M.A.; Wang, G.; Hill, A.D.; Nasr-El-Din, H.A. Acid diversion by use of viscoelastic surfactants: The effects of flow rate and initial permeability contrast. *SPE J.* **2014**, *19*, 1203–1216. [CrossRef]
25. Huang, T.; Hill, A.; Schechter, R. Reaction rate and fluid loss: The keys to wormhole initiation and propagation in carbonate acidizing. *SPE J.* **2000**, *5*, 287–292. [CrossRef]

Disclaimer/Publisher's Note: The statements, opinions and data contained in all publications are solely those of the individual author(s) and contributor(s) and not of MDPI and/or the editor(s). MDPI and/or the editor(s) disclaim responsibility for any injury to people or property resulting from any ideas, methods, instructions or products referred to in the content.